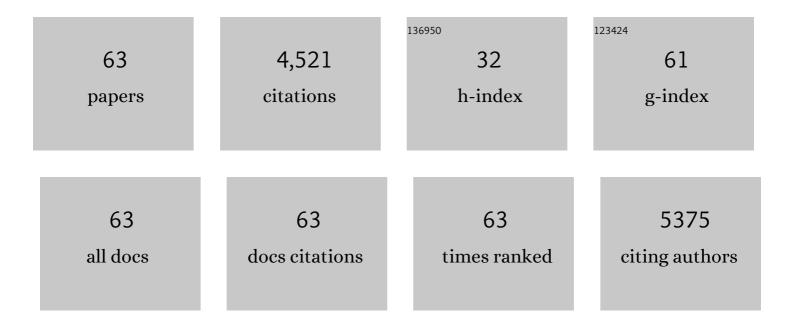
Young-Sang Yu

List of Publications by Year in descending order

Source: https://exaly.com/author-pdf/2655898/publications.pdf Version: 2024-02-01



YOUNG-SANG YU

#	Article	IF	CITATIONS
1	Correlative analysis of structure and chemistry of LixFePO4 platelets using 4D-STEM and X-ray ptychography. Materials Today, 2022, 52, 102-111.	14.2	4
2	Correlative image learning of chemo-mechanics in phase-transforming solids. Nature Materials, 2022, 21, 547-554.	27.5	27
3	4D Imaging of ZnO-Coated Nanoporous Al ₂ O ₃ Aerogels by Chemically Sensitive Ptychographic Tomography: Implications for Designer Catalysts. ACS Applied Nano Materials, 2021, 4, 621-632.	5.0	14
4	Unlocking anionic redox activity in O3-type sodium 3d layered oxides via Li substitution. Nature Materials, 2021, 20, 353-361.	27.5	155
5	Cation ordered Ni-rich layered cathode for ultra-long battery life. Energy and Environmental Science, 2021, 14, 1573-1583.	30.8	83
6	Fictitious phase separation in Li layered oxides driven by electro-autocatalysis. Nature Materials, 2021, 20, 991-999.	27.5	101
7	Differential electron yield imaging with STXM. Ultramicroscopy, 2021, 222, 113198.	1.9	2
8	Topology-dependent stability of vortex-antivortex structures. Applied Physics Letters, 2021, 118, .	3.3	8
9	Correlative operando microscopy of oxygen evolution electrocatalysts. Nature, 2021, 593, 67-73.	27.8	321
10	Persistent and partially mobile oxygen vacancies in Li-rich layered oxides. Nature Energy, 2021, 6, 642-652.	39.5	106
11	Soft x-ray linear dichroic ptychography: the study of crystal orientation in biominerals. , 2021, , .		2
12	Lessons learned from FeSb2O4 on stereoactive lone pairs as a design principle for anion insertion. Cell Reports Physical Science, 2021, 2, 100592.	5.6	3
13	A tailored oxide interface creates dense Pt single-atom catalysts with high catalytic activity. Energy and Environmental Science, 2020, 13, 1231-1239.	30.8	140
14	Mapping Competitive Reduction upon Charging in LiNi _{0.8} Co _{0.15} Al _{0.05} O ₂ Primary Particles. Chemistry of Materials, 2020, 32, 6161-6175.	6.7	5
15	Reversible Room-Temperature Fluoride-Ion Insertion in a Tunnel-Structured Transition Metal Oxide Host. ACS Energy Letters, 2020, 5, 2520-2526.	17.4	13
16	A highly stabilized Ni-rich NCA cathode for high-energy lithium-ion batteries. Materials Today, 2020, 36, 73-82.	14.2	163
17	An ultrahigh-resolution soft x-ray microscope for quantitative analysis of chemically heterogeneous nanomaterials. Science Advances, 2020, 6, .	10.3	47
18	Multimodal x-ray and electron microscopy of the Allende meteorite. Science Advances, 2019, 5, eaax3009.	10.3	17

YOUNG-SANG YU

#	Article	IF	CITATIONS
19	Quantification of Heterogeneous Degradation in Liâ€lon Batteries. Advanced Energy Materials, 2019, 9, 1900674.	19.5	176
20	Intercalation of Magnesium into a Layered Vanadium Oxide with High Capacity. ACS Energy Letters, 2019, 4, 1528-1534.	17.4	75
21	Dynamics of the Bloch point in an asymmetric permalloy disk. Nature Communications, 2019, 10, 593.	12.8	33
22	The Hydration of β- and α′ _H -Dicalcium Silicates: An X-ray Spectromicroscopic Study. ACS Sustainable Chemistry and Engineering, 2019, 7, 2316-2326.	6.7	42
23	Probing the Location and Speciation of Elements in Zeolites with Correlated Atom Probe Tomography and Scanning Transmission Xâ€Ray Microscopy. ChemCatChem, 2019, 11, 488-494.	3.7	19
24	The chemistry and structure of calcium (alumino) silicate hydrate: A study by XANES, ptychographic imaging, and wide- and small-angle scattering. Cement and Concrete Research, 2019, 115, 367-378.	11.0	104
25	Advanced denoising for X-ray ptychography. Optics Express, 2019, 27, 10395.	3.4	18
26	Multivalent Electrochemistry of Spinel Mg _{<i>x</i>} Mn _{3–<i>x</i>} O ₄ Nanocrystals. Chemistry of Materials, 2018, 30, 1496-1504.	6.7	23
27	Three-dimensional localization of nanoscale battery reactions using soft X-ray tomography. Nature Communications, 2018, 9, 921.	12.8	107
28	Dataflow at the COSMIC Beamline - Stream Processing and Supercomputing. Microscopy and Microanalysis, 2018, 24, 58-59.	0.4	4
29	Automatic projection image registration for nanoscale X-ray tomographic reconstruction. Journal of Synchrotron Radiation, 2018, 25, 1819-1826.	2.4	23
30	Fluid-enhanced surface diffusion controls intraparticle phase transformations. Nature Materials, 2018, 17, 915-922.	27.5	104
31	Synchrotron X-ray nanotomographic and spectromicroscopic study of the tricalcium aluminate hydration in the presence of gypsum. Cement and Concrete Research, 2018, 111, 130-137.	11.0	79
32	Removal of Hexavalent Chromium in Portland Cement Using Ground Granulated Blast-Furnace Slag Powder. Materials, 2018, 11, 11.	2.9	31
33	The COSMIC Imaging Beamline at the Advanced Light Source: a new facility for spectro-microscopy of nano-materials. Microscopy and Microanalysis, 2018, 24, 8-11.	0.4	12
34	Understanding Chemomechanical Li-ion Cathode Degradation through Multi-Scale, Multi-Modal X-ray Spectromicroscopy. Microscopy and Microanalysis, 2018, 24, 426-427.	0.4	2
35	Near-edge X-ray refraction fine structure microscopy. Applied Physics Letters, 2017, 110, .	3.3	39
36	Simultaneous control of magnetic topologies for reconfigurable vortex arrays. NPG Asia Materials, 2017, 9, e348-e348.	7.9	18

#	ARTICLE Nanometer-Resolved Spectroscopic Study Reveals the Conversion Mechanism of	IF	CITATIONS
37	CaO·Al ₂ O ₃ ·10H ₂ O to 2CaO·Al ₂ O ₃ ·8H ₂ O and 3CaO·Al ₂ O ₃ ·6H ₂ O at an Elevated Temperature. Crystal Growth	3.0	44
38	Intergranular Cracking as a Major Cause of Long-Term Capacity Fading of Layered Cathodes. Nano Letters, 2017, 17, 3452-3457.	9.1	361
39	Using Scanning Transmission X-ray Microscopy to Reveal the Origin of Lithium Compositional Spatiodynamics in Battery Materials. Microscopy and Microanalysis, 2017, 23, 888-889.	0.4	0
40	Nanoscale Detection of Intermediate Solid Solutions in Equilibrated Li _{<i>x</i>/i>} FePO ₄ Microcrystals. Nano Letters, 2017, 17, 7364-7371.	9.1	27
41	Ptychographic Imaging of Nano-Materials at the Advanced Light Source with the Nanosurveyor Instrument. Journal of Physics: Conference Series, 2017, 849, 012028.	0.4	15
42	Robust X-Ray Phase Ptycho-Tomography. IEEE Signal Processing Letters, 2016, 23, 944-948.	3.6	14
43	Origin and hysteresis of lithium compositional spatiodynamics within battery primary particles. Science, 2016, 353, 566-571.	12.6	367
44	Visualization of the Phase Propagation within Carbon-Free Li4Ti5O12 Battery Electrodes. Journal of Physical Chemistry C, 2016, 120, 29030-29038.	3.1	10
45	The Formation Mechanism of Fluorescent Metal Complexes at the Li _{<i>x</i>} Ni _{0.5} Mn _{1.5} O _{4â^'δ} /Carbonate Ester Electrolyte Interface. Journal of the American Chemical Society, 2015, 137, 3533-3539.	13.7	182
46	Dependence on Crystal Size of the Nanoscale Chemical Phase Distribution and Fracture in Li _{<i>x</i>} FePO ₄ . Nano Letters, 2015, 15, 4282-4288.	9.1	99
47	Nonequilibrium Pathways during Electrochemical Phase Transformations in Single Crystals Revealed by Dynamic Chemical Imaging at Nanoscale Resolution. Advanced Energy Materials, 2015, 5, 1402040.	19.5	42
48	Visualization of electrochemically driven solid-state phase transformations using operando hard X-ray spectro-imaging. Nature Communications, 2015, 6, 6883.	12.8	80
49	Direct Observation of Reversible Magnesium Ion Intercalation into a Spinel Oxide Host. Advanced Materials, 2015, 27, 3377-3384.	21.0	178
50	Chemical composition mapping with nanometre resolution by soft X-ray microscopy. Nature Photonics, 2014, 8, 765-769.	31.4	371
51	Resonant amplification of vortex-core oscillations by coherent magnetic-field pulses. Scientific Reports, 2013, 3, 1301.	3.3	13
52	Logic Operations Based on Magnetic-Vortex-State Networks. ACS Nano, 2012, 6, 3712-3717.	14.6	84
53	Memory-bit selection and recording by rotating fields in vortex-core cross-point architecture. Applied Physics Letters, 2011, 98, .	3.3	60
54	Polarization-selective vortex-core switching by tailored orthogonal Gaussian-pulse currents. Physical Review B, 2011, 83, .	3.2	13

YOUNG-SANG YU

#	Article	IF	CITATIONS
55	Observation of coupled vortex gyrations by 70-ps-time- and 20-nm-space-resolved full-field magnetic transmission soft x-ray microscopy. Applied Physics Letters, 2010, 97, .	3.3	47
56	Out-of-plane current controlled switching of the fourfold degenerate state of a magnetic vortex in soft magnetic nanodots. Applied Physics Letters, 2010, 96, 072507.	3.3	39
57	Low-Power Selective Control of Ultrafast Vortex-Core Switching by Circularly Rotating Magnetic Fields: Circular–Rotational Eigenmodes. IEEE Transactions on Magnetics, 2008, 44, 3071-3074.	2.1	15
58	Understanding eigenfrequency shifts observed in vortex gyrotropic motions in a magnetic nanodot driven by spin-polarized out-of-plane dc current. Applied Physics Letters, 2008, 93, .	3.3	30
59	Reliable low-power control of ultrafast vortex-core switching with the selectivity in an array of vortex states by in-plane circular-rotational magnetic fields and spin-polarized currents. Applied Physics Letters, 2008, 92, .	3.3	159
60	Oppositely rotating eigenmodes of spin-polarized current-driven vortex gyrotropic motions in elliptical nanodots. Applied Physics Letters, 2008, 92, .	3.3	13
61	Universal Criterion and Phase Diagram for Switching a Magnetic Vortex Core in Soft Magnetic Nanodots. Physical Review Letters, 2008, 101, 267206.	7.8	104
62	An interface-proximity model for switchable interfacial uncompensated antiferromagnetic spins and their role in exchange bias. Applied Physics Letters, 2005, 86, 192512.	3.3	5
63	Vortex–antivortex pair driven magnetization dynamics studied by micromagnetic simulations. Applied Physics Letters, 2004, 85, 1568-1570.	3.3	29